Supporting Information

A novel bright cyan emitting phosphor of Eu^{2+} activated $Ba_6BO_3Cl_9$ with robust thermal stability for full-spectrum WLED applications

Shengjian Jiao,[a,b] Ran Pang,[a,*] Jiutian Wang,[a,b] Tao Tan,[a,b] Chengyu Li,[a,b,*] and Hongjie Zhang[a,c]

[a] *State key Laboratory of Rare Earth Resource Utilization, Changchun Institute of Applied Chemistry, Chinese Academy of Sciences, Changchun 130022, China*

[b] *University of Science and Technology of China, Hefei 230026, China*

[c] *The GBA National Institute for Nanotechnology Innovation, Guangzhou 510535, China*

** Corresponding author: Tel: +86-0431-85262258*

E-mail address: cyli@ciac.ac.cn and pangran@ciac.ac.cn

Table S1 Rietveld fitting results of BBC and BBC: $0.05Eu^{2+}$

formula	BBC	BBC: $0.05Eu^{2+}$
crystal system	monoclinic	monoclinic
space group	$P2_1/c$	$P2_1/c$
a (Å)	8.2466(2)	8.2442(7)
b (Å)	12.2685(2)	12.2676(1)
c (Å)	19.1109(3)	19.1157(2)
$\alpha = \beta = \gamma$(deg)	90	90
Z	4	4
V (Å^3)	1933.51(7)	1933.3(5)
R_p	0.0292	0.0619
R_{wp}	0.0376	0.0941
χ^2	1.875	2.543

Table S2 Atomic positions of $Ba_6BO_3Cl_9$

atom	site	x	y	z	occupancy	U_{iso}
Ba1	4e	-0.05149	0.17482	0.50470	1.000	0.01496
Ba2	4e	-0.06280	0.17843	0.24430	1.000	0.01857
Ba3	4e	0.42654	0.33286	0.50219	1.000	0.01619
Ba4	4e	0.42583	0.32508	0.25090	1.000	0.02474
Ba5	4e	0.45877	0.04872	0.37226	1.000	0.01588
Ba6	4e	-0.05581	0.46467	0.37458	1.000	0.01190
B	4e	0.16239	0.28865	0.34253	1.000	-0.05952
O1	4e	0.12304	0.29624	0.42315	1.000	-0.06064
O2	4e	0.13589	0.2923	0.26258	1.000	0.01568
O3	4e	0.33079	0.25664	0.36404	1.000	-0.04351
Cl1	4e	-0.07419	0.00138	0.62518	1.000	-0.00313
Cl2	4e	-0.20837	0.45066	0.52714	1.000	0.00228
Cl3	4e	-0.1395	0.71509	0.37508	1.000	-0.00751
Cl4	4e	-0.17233	0.44221	0.23637	1.000	-0.00996
Cl5	4e	-0.0436	-0.01923	0.13443	1.000	-0.00844
Cl6	4e	0.27648	0.08211	0.22565	1.000	-0.01231
Cl7	4e	0.72565	0.23162	0.36609	1.000	-0.00607
Cl8	4e	0.71647	-0.06505	0.4826	1.000	-0.01644
Cl9	4e	0.36492	-0.18846	0.38465	1.000	0.01505

Table S3 Atomic positions of $Ba_6BO_3Cl_9$: $0.05Eu^{2+}$

atom	site	x	y	z	occupancy	U_{iso}
Ba1	4e	-0.05246	0.17373	0.50652	0.9844	0.01291
Ba2	4e	-0.06265	0.17968	0.24271	0.9829	0.02173
Ba3	4e	0.42634	0.33187	0.50248	0.9505	0.01428
Ba4	4e	0.42763	0.32501	0.24925	0.9475	0.03047
Ba5	4e	0.45823	0.04871	0.37113	0.934	0.01469
Ba6	4e	-0.05395	0.46527	0.37396	0.9007	0.00921
Eu1	4e	-0.05246	0.17373	0.50652	0.0156	0.02295
Eu2	4e	-0.06265	0.17968	0.24271	0.0171	0.02816
Eu3	4e	0.42634	0.33187	0.50248	0.0495	0.02308
Eu4	4e	0.42763	0.32501	0.24925	0.0525	0.03073
Eu5	4e	0.45823	0.04871	0.37113	0.066	0.02381
Eu6	4e	-0.05395	0.46527	0.37396	0.0993	0.02231
B	4e	0.14513	0.28157	0.35263	1.000	-0.02022
O1	4e	0.11471	0.30256	0.42414	1.000	-0.03851
O2	4e	0.15588	0.29597	0.22045	1.000	0.14075
O3	4e	0.34029	0.25868	0.37112	1.000	-0.05713
Cl1	4e	-0.07477	-0.00008	0.61792	1.000	0.00273
Cl2	4e	-0.21793	0.45238	0.52767	1.000	0.01774
Cl3	4e	-0.13811	0.7196	0.37924	1.000	-0.02578
Cl4	4e	-0.17952	0.44792	0.23369	1.000	-0.00902
Cl5	4e	-0.04115	-0.01931	0.13526	1.000	0.00626
Cl6	4e	0.27585	0.08028	0.22688	1.000	-0.00782
Cl7	4e	0.72385	0.23778	0.37216	1.000	-0.00996
Cl8	4e	0.71205	-0.06391	0.48177	1.000	-0.01664
Cl9	4e	0.36667	-0.18984	0.37874	1.000	0.03524

Table S4 Bond details of Ba-O and Ba-Cl in the BBC and BBC: $0.05Eu^{2+}$

Bond	BBC	BBC: $0.05Eu^{2+}$
$Ba1\text{-}Cl1_{I}$	3.1409	3.0190
$Ba1\text{-}Cl1_{II}$	3.4519	3.3609
Ba1-Cl2	3.6485	3.7027
Ba1-Cl3	3.0940	2.9918
Ba1-Cl7	3.2965	3.2583
$Ba1\text{-}Cl8_{I}$	3.5353	3.5344
$Ba1\text{-}Cl8_{II}$	3.0827	3.1211
Ba1-Cl9	3.3460	3.3998
Ba1-O1	2.5935	2.6223
Ba2-Cl1	3.5151	3.6382
Ba2-Cl3	3.3791	3.4296
$Ba2\text{-}Cl4_{I}$	3.3633	3.4332
$Ba2\text{-}Cl4_{II}$	3.6480	3.5784
Ba2-Cl5	3.2117	3.1952
Ba2-Cl6	3.0585	3.0604
Ba2-Cl7	2.9829	3.1190
Ba2-Cl9	3.3785	3.2499
Ba2-O2	2.1810	2.3371
$Ba3\text{-}Cl2_{I}$	3.3729	3.3195
$Ba3\text{-}Cl2_{II}$	3.2561	3.2078
Ba3-Cl3	3.3863	3.3400
$Ba3\text{-}Cl5_{I}$	3.3239	3.3408
$Ba3\text{-}Cl5_{II}$	3.4167	3.4353
Ba3-Cl8	3.5032	3.4925
Ba3-Cl9	3.2807	3.3321
Ba3-O1	2.9558	2.9956
Ba3-O3	2.9089	2.7597
Ba4-Cl1	3.2103	3.3039
Ba4-Cl3	3.2763	3.2733
Ba4-Cl4	3.6230	3.5848
Ba4-Cl5	3.0640	3.0656
$Ba4\text{-}Cl6_{I}$	3.2609	3.2806
$Ba4\text{-}Cl6_{II}$	3.5959	3.5817
Ba4-Cl9	3.5312	3.4508
Ba4-O2	2.4352	2.3344
Ba4-O3	2.4494	2.5705
Ba5-Cl1	3.2309	3.2239
Ba5-Cl4	3.0216	2.9784

Ba5-Cl6	3.2040	3.1646
Ba5-Cl7	3.1455	3.1899
Ba5-$Cl8_{I}$	3.3012	3.2806
Ba5-$Cl8_{II}$	3.1358	3.1482
Ba5-Cl9	3.0204	3.0257
Ba5-O3	2.7649	2.7532
Ba6-$Cl2_{I}$	3.1818	3.2380
Ba6-$Cl2_{II}$	3.0564	3.0954
Ba6-Cl3	3.1488	3.1978
Ba6-Cl4	2.8228	2.8822
Ba6-Cl5	3.3136	3.3481
Ba6-Cl6	3.3263	3.3108
Ba6-Cl7	3.3835	3.3385
Ba6-O1	2.7025	2.6151
Ba6-O2	3.4004	3.3054

Table S5 Average lifetime (τ) of Eu^{2+} 470 nm emission in BBC: xEu^{2+}phosphors (under 375 nm excitation)

Eu(x)	A_1	τ_1	A_2	τ_2	τ_{ave} (ns)
0.01	1876.968	394.1397	5291.57	699.5588	648.688
0.02	1496.992	293.6175	5898.081	682.9566	644.6523
0.03	1227.002	267.8218	6287.244	672.9735	643.4022
0.04	1360.158	252.7384	6171.785	672.9735	640.851
0.05	1293.494	184.6729	6401.28	662.0272	636.5559
0.06	1533.895	226.095	6155.831	663.3228	629.0949
0.07	1749.579	172.4845	6343.757	659.4066	627.643
0.08	1763.353	215.9969	6227.862	663.9352	626.1543
0.09	1510.143	190.1002	6188.861	656.7849	625.999
0.10	1543.166	195.2316	6059.367	653.167	620.7738

Table S6. The detail information of Gaussian sub-bands of $Ba_6BO_3Cl_9$: $0.05Eu^{2+}$ sample measured at liquid helium temperature.

Wavelength (nm)	Wavenumber (cm^{-1})	Area proportion (%)	FWHM (nm)
457	21,882	10.88	23.76
470	21,276	34.09	39.40
496	20,161	33.07	61.02
522	19,157	21.95	106.13

Table S7. Total energy and defect formation energy of BBC: Eu_{Ba}.

Compositions	E(doped) (eV)	E(undoped) (eV)	E_f (eV)
BBC: Eu_{Ba1}	-397.750	-397.622	7.932
BBC: Eu_{Ba3}	-397.926	-397.622	7.756
BBC: Eu_{Ba5}	-397.992	-397.622	7.690
BBC: Eu_{Ba6}	-398.000	-397.622	7.682

Table S8. The CIE coordinates of BBC: $0.05Eu^{2+}$ phosphors under the excitation of 355 nm at different temperature (298 K - 573 K).

Temperature (°C)	CIE coordinates	Peak (nm)
25	(0.1673, 0.2393)	470
50	(0.1693, 0.2384)	469
75	(0.1712, 0.2376)	468
100	(0.1733, 0.2380)	468
125	(0.1751, 0.2383)	468
150	(0.1771, 0.2397)	468
175	(0.1789, 0.2404)	464
200	(0.1806, 0.2411)	468
225	(0.1824, 0.2410)	468
250	(0.1836, 0.2407)	466
275	(0.1851, 0.2410)	468
300	(0.1868, 0.2412)	467

Table S9. Comparation of luminescence properties of BBC:0.05Eu^{2+} and some reported blue and cyan phosphors.

Phosphor	Peak position (nm)	FWHM (nm)	IQE (%)	EQE (%)	I_{150}℃ (%)	Ref.
$Na_{0.2}Al_2B_2O_7$: 1.8Eu	470	~70	60.2	24.9	83	1
$Na_{0.5}K_{0.5}Li_3SiO_4$: Eu^{2+}	486	20.7	76	30	93	2
$BaAl_{12}O_{19}$: Eu^{2+}	445	52	89.6	/	91.1	3
$Ba_{0.98}ScO_2F$: 0.02Eu^{2+}	487	103	~80	/	~30	4
$ScCaO(BO_3)$: Ce^{3+}	473	97	66.5	38.5	21.5	5
$BaScO_2F$: Bi^{3+}, K^+	506	~50	57.3		87	6
$Ca_3Ga_4O_9$: 0.02Bi^{3+}, 0.07Zn^{2+}	486	99	51.5	39.2	76	7
$Ca_2LuZr_2(AlO_4)_3$: Ce^{3+}	483	84	58	/	67	8
$SrLaGaO_4$: Bi^{3+}	475	107	/	/	~15	9
$Ca_2GdHf_2(AlO_4)_3$: Ce^{3+}	489	103	80	49	/	10
$NaMgBO_3$: Ce^{3+}	480	102	/	/	~80	11
$Ba_2CaB_2Si_4O_{14}$: Ce^{3+}	478	142	54	/	95	12
$Ba_6BO_3Cl_9$:Eu^{2+}	470	59.84	86.2	41.3	93.9	This work

Table S10. Full set of 15 CRIs and the average CRI (Ra) values of the as-prepared WLEDs.

CRIs	R1	R2	R3	R4	R5	R6	R7	R8	R9	R10	R11	R12	R13	R14	R15	Ra
LED_1	71	72	85	81	69	63	89	87	50	48	75	39	68	94	64	77.1
LED_2	96	98	98	96	97	97	92	84	59	96	97	96	96	99	92	94.8
LED_3	81	85	93	81	80	84	91	70	14	69	80	66	81	97	70	83
LED_4	81	88	96	82	82	82	97	89	70	75	75	78	81	97	83	87.2
LED_5	97	97	96	94	97	95	99	96	84	95	90	94	98	97	96	96.4
LED_6	95	91	88	81	92	91	82	81	63	84	86	79	91	94	84	87.7
LED_7	25	58	30	8	43	53	50	21	-194	23	-5	53	28	57	22	35.9

Figures and Figure Captions

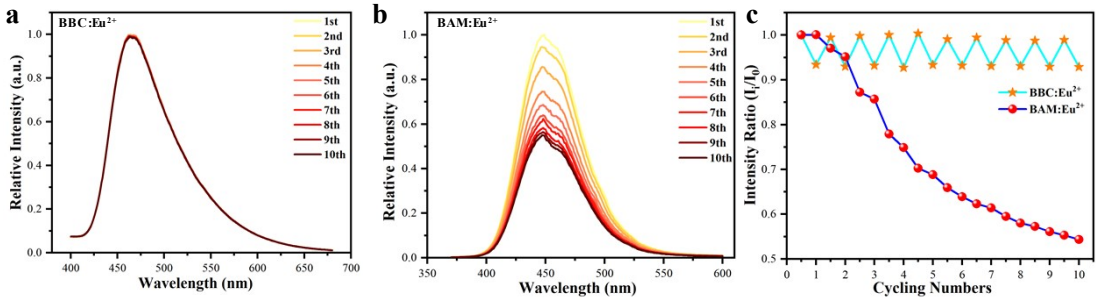

Figure S1 (a) Normalized spectra of BBC: Eu^{2+} measured at 150 °C upon 355 nm excitation for consecutive ten thermocycling. **(b)** Normalized spectra of BAM: Eu^{2+} measured at 150 °C upon 365 nm excitation for consecutive ten thermocycling. **(c)** Reversible temperature-sensing performance of BBC: Eu^{2+} and BAM: Eu^{2+}based on the integral intensity in heating–cooling cycles.

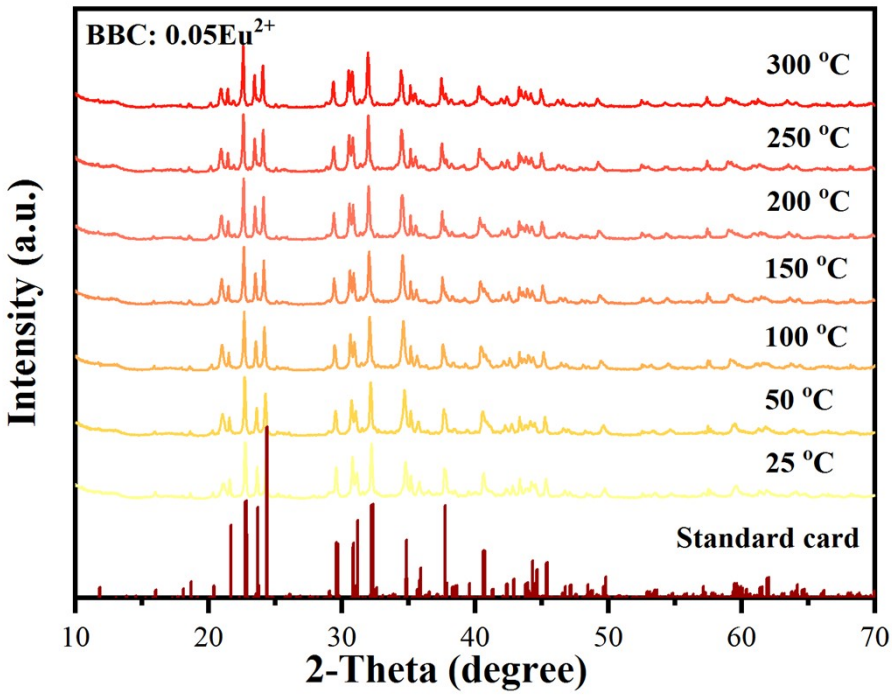

Figure S2 Temperature dependent XRD patterns of BBC: 0.05Eu^{2+} samples in 2θ range of 10 — 70°.

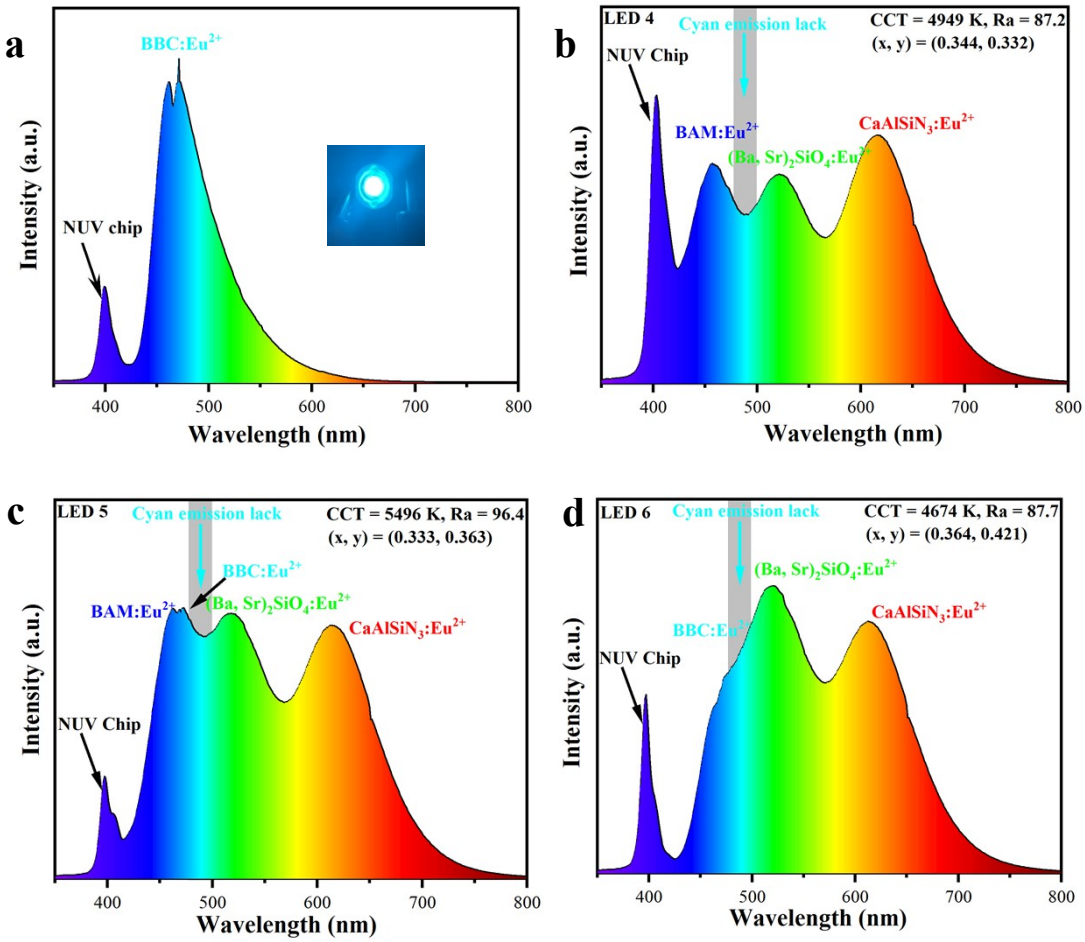

Figure S3 The PL spectrum of fabricated full spectrum w-LEDs based on the strategies of RGB phosphors combined with 395 nm-emitting InGaN chip.

Supplementary Notes

Supplementary Note 1:

The Kubelka–Munk function is used herein,[3, 13, 14] which can be expressed as:

$$\left[F(R_\infty)hv\right]^n = C(hv - E_g) \quad (1)$$

where hv is the photon energy, A is the absorption constant, E_g is the value of the band gap, n represents the transition coefficient (n = 2 for the direct band gap, n = 1/2 for the indirect band gap), $F(R_\infty)$ is the Kubelka–Munk function, which is calculated by the following equation:[3, 15]

$$\left[F(R_\infty)\right] = (1 - R)^2 \,/\, 2R \quad (2)$$

In the above equation, R is the reflectance parameter in the DRS.

Supplementary Note 2:

To investigate the mechanism of concentration quenching for Eu^{2+}-doped BBC, the critical distance Rc for qualitatively judging non-radiative energy transfer between the Eu^{2+} ions in the host lattice can be calculated using the formula proposed by Blass Grabmaier, as follows: [14, 16, 17]

$$R_C \approx 2\left[\frac{3V}{4\pi X_C Z}\right]^{1/3} \quad (3)$$

where V represents the volume of host lattice, X_C is the critical value of the concentration, and Z denotes the number of sites in the unit cell that can be doped. For the BBC crystal structure, V = 638.23(31) $Å^3$, X_C = 0.05, and Z = 4, so the critical distance R_c of Eu^{2+} ions was calculated to be approximately 18.27 Å. As is known to all, the exchange interaction is a short-range effect that occurs only when the distance between activators is less than 5 Å. Therefore, the exchange interaction can be excluded. Hence, we speculate that electric multipolar-multipolar interaction plays a major role in the concentration quenching for BBC: Eu^{2+}. According to the report of Van Uiter and Dexter, the emission intensity per activators can be expressed by the following equation:[17, 18]

$$\frac{I}{x} = \frac{k}{1+\beta(x)^{\theta/3}} \quad (4)$$

where I represents the luminescence intensity, x denotes the optimum concentration of the activator ions, k and β are constants for a given host lattice and excitation conditions, and θ offers an indication of electric multipolar nature. When θ is equal to 6, 8 or 10, it corresponds to dipole-dipole (d-d), dipole-quadrupole (d-q) and quadrupole-quadrupole (q-q) interactions, respectively. $\theta = 3$ denotes energy migration between the closest or next closest Eu^{2+} ions. As depicted in the inset of Fig. 3e, the dependence of Ln (I/x) and Ln (x) can be well-fitted as a line with the slope 2.653, and the θ can be calculated to be approximately 7.89, which is close to 8. The finding suggests that dipole-quadrupole interaction is the major mechanism type of concentration quenching behavior for BBC: xEu^{2+} phosphors.

Supplementary Note 3:

The average decay time of the sample can be computed as follows:[19-21]

$$I = \sum_{i=1}^{n} A_i exp\left(-t/\tau_i\right) \quad (5)$$

$$\tau_{ave} = \frac{\sum_{i=1}^{n} A_i \tau_i^2}{\sum_{i=1}^{n} A_i \tau_i} \quad (6)$$

where I is the luminescence intensity, A_i is constant, t is the time, and τ_i is the decay time for the every components, respectively. Therefore, the average lifetimes of BBC: xEu^{2+} ($0.01 \leq x \leq 0.10$) were calculated to be 648.69, 643.40, 636.55, 627.64, 625.99 and 620.77 ns for x values of 0.01, 0.03, 0.05, 0.07, 0.09, 0.10, respectively. The detailed calculation results are listed in the Table S5. The fitting result is within the usual time range of the spin-allowed $4f^6 5d^1 \rightarrow 4f^7$ ($^8S_{7/2}$) of Eu^{2+}.

Supplementary Note 4:

We roughly estimate the relationship between the luminescence centers of Eu^{2+} and local structure of cationic sites according to the empirical formula established by Van Uitert:[2, 14, 22]

$$E = Q\left[1 - \left(\frac{V}{4}\right)^{\frac{1}{V}} \times 10^{-\frac{nEar}{80}}\right] \quad (7)$$

where, E (cm^{-1}) represents the energy position of Eu^{2+} emission peak; Q stands for the energy position for the lowest d-band edge for free ion ($Q_{Eu^{2+}}$ = 34 000 cm^{-1}); V is the valence of the cation ($V_{Eu^{2+}}$ = 2); n is the coordination number (CN) of the site occupied by activator ion; Ea refers to the electron affinity (eV) of anion atom, which is a constant in the same host; and r is the radius of the cationic ion ($r_{Ba^{2+}} = 1.42, CN = 8$), ($r_{Ba^{2+}} = 1.47, CN = 9$) replaced by the activator (Eu^{2+}). It is not practical to accurately obtain the emission position (E). However, considering that E is proportional to the product of n and r, we can qualitatively judge which crystallographic site is replaced by Eu^{2+} in BBC host.

Supplementary Note 5:

Generally, the crystal field splitting of the $4f^{n-1}5d$-levels of Ce^{3+} and Eu^{2+} (ε_{cfs}) is a good index to evaluate the site occupations of activator ions, which is closely related to coordination number, polyhedron shape and size, while being irrelevant of the anion types.[23, 24] According to the theory of Dorenbos, the crystal field splitting ε_{cfs} can be evaluated by the following equation:[25, 26]

$$\varepsilon_{cfs} = \beta_{poly}^{Q} R_{av}^{-2} \tag{8}$$

where β_{poly}^{Q} is a constant depends on the type of coordination polyhedron, irrespective of the lanthanide valence (trivalent, Q=3+ or divalent, Q=2+). R_{av} is defined as

$$R_{av} = \frac{1}{N}\sum_{i=1}^{N}(R_i - 0.6\Delta R) \tag{9}$$

where R_i are the individual bond length to the N coordinating anions in the unrelaxed lattice. $\Delta R \equiv R_M - R_{Ln}$, where R_M is the ionic radius of the cation which is replaced by the lanthanide Ln with ionic radius R_{Ln}. $0.6\Delta R$ is an estimation of the bond length relaxation. When the polyhedron occupied by Eu^{2+} ions have the same shape, the β_{poly}^{Q} has no influence on ε_{cfs}. In this case, the crystal field splitting ε_{cfs} is closely related to the bond length. It can be seen that the short bond length means bigger degree of crystal field splitting and a longer emission wavelength. However, when the polyhedron occupied by Eu^{2+} ions have different shape, it is necessary to compare the influence between β_{poly}^{Q} and R_{av}^{-2}. In general, polyhedron with higher coordination number tends to reduce the crystal field splitting. When the coordination numbers are same but the shape are different, the ε_{cfs} of polyhedrons is mainly depend on R_{av}^{-2}.

Supplementary Note 6:

To better comprehend thermal quenching, a modified Arrhenius equation can be used to represent the relationship between the temperature and the emission intensity.[27-29]

$$I(T) = \frac{I_0}{1 + A \cdot exp\left(-\frac{\Delta E}{k_B \cdot T}\right)} \quad (10)$$

where I_0 represents the initial emission intensity (298 K), $I(T)$ denotes the luminescence intensity at a specified temperature T, A is the constant, and k_B is Boltzmann constant (8.617×10^{-5} eV/K). As is shown in Fig. 6c，we can obtain the relationship of ln (I_0/I_T -1) with $1/k_BT$ is linear with the slope value of $-E_a$. From the fitting result of Fig. 6c, it is confirmed that ΔE is equal to 0.3612 eV for the BBC: $0.05Eu^{2+}$ phosphor.

Supplementary Note 7:

The chromaticity shift (ΔE_s) can efficiently evaluate the chromaticity stability of phosphor, which can be calculated by the following equation:[5, 30, 31]

$$\Delta E_s = \sqrt{\left(u_t^{'} - u_{298K}^{'}\right)^2 + \left(v_t^{'} - v_{298K}^{'}\right)^2 + \left(w_t^{'} - w_{298K}^{'}\right)^2} \quad (11)$$

where *u'* = *4x*/(*3-2x+12y*), *v'* = *9y*/(*3-2x+12y*) and *w'* = 1-*u'*-*v'*. The *x* and *y* are chromaticity coordinates in CIE 1931 color space, and *t* is the given temperature. ΔE_s of the representative BBC: $0.05Eu^{2+}$ phosphor at 150 °C was determined as 1.18×10^{-2}, which was smaller than commercial $BaMgAl_{10}O_{17}:Eu^{2+}$ blue phosphor (ΔE_s = 1.52×10^{-2}),[32] commercial $CaAlSiN_3:Eu^{2+}$ red phosphor ($\Delta E_s = 4.4\times10^{-2}$),[33] and some phosphor reported recently such as $Ca_2LuHf_2Al_3O_{12}:Ce^{3+}$ cyan phosphor (ΔE_s = 1.7×10^{-2}),[34] $CaGd_2HfSc(AlO_4)_3:Ce^{3+}$ yellow phosphor (ΔE_s = 2.1×10^{-2}),[35] $CsMoO_2F_3:Mn^{4+}$ red phosphor ($\Delta E_s = 3.39\times10^{-2}$),[36] etc.

Supplementary Note 8:

The Debye temperature has recently been proven to be a proxy of structural rigidity, which can be calculated based on the following equation: [6, 31, 37]

$$\Theta_D = \sqrt{\frac{3h^2TN_A}{Ak_BU_{iso}}} \quad (12)$$

where Θ_D is negative relation with average atomic displacement parameter (U_{iso}). The Debye temperature of BBC was calculated by the DFT-PBE method, the calculation result is 517 K. The calculated Θ_D value for $Sr_3(PO_4)_2$: Eu^{2+} is 559 K, the recently reported superb thermal stability phosphor with emission loss of only 4%/8% at 150/300 °C.[38] The Θ_D value for $SrGa_2B_2O_7$: Bi^{3+} with negative thermal quenching is 602 K, which keeps 124.8% emission intensity of initial intensity at 150 °C.[39] In addition, the calculated Θ_D of $(Ba_{1-x}Sr_x)_{0.98}Eu_{0.02}ScO_2F$ phosphor host with excellent thermal stability is 497 K.[4]

Supplementary Note 9:

The internal quantum efficiencies (IQE) can be calculated based on the following equation:[21, 40]

$$\eta_{IQE} = \frac{\int L_S}{\int E_R - \int E_S} \quad (13)$$

where LS represents PL spectrum of the sample. ES is the excitation spectrum used to excite samples. ER is the spectrum of the excitation light without sample in the integrating sphere.

Reference

1. X. Zhang, J. Zhang, X. Wu, L. Yu, Y. Liu, X. Xu and S. Lian, Discovery of blue-emitting Eu2+-activated sodium aluminate phosphor with high thermal stability via phase segregation, *Chem. Eng. J.*, 2020, **388**, 124289.
2. M. Zhao, H. Liao, M. S. Molokeev, Y. Zhou, Q. Zhang, Q. Liu and Z. Xia, Emerging ultra-narrow-band cyan-emitting phosphor for white LEDs with enhanced color rendition, *Light Sci Appl*, 2019, **8**, 38.
3. Y. Wei, L. Cao, L. Lv, G. Li, J. Hao, J. Gao, C. Su, C. C. Lin, H. S. Jang, P. Dang and J. Lin, Highly Efficient Blue Emission and Superior Thermal Stability of $BaAl_{12}O_{19}:Eu^{2+}$ Phosphors Based on Highly Symmetric Crystal Structure, *Chem. Mater.*, 2018, **30**, 2389-2399.
4. S. Hariyani, M. Amachraa, M. Khan, S. P. Ong and J. Brgoch, Local environment rigidity and the evolution of optical properties in the green-emitting phosphor $Ba_{1-x}Sr_xScO_2F:Eu^{2+}$, *J. Mater. Chem. C*, 2022, **10**, 2955-2964.
5. W. Wang, T. Tan, S. Wang, S. Zhang, R. Pang, D. Li, L. Jiang, H. Li, C. Li and H. Zhang, Low-concentration Ce^{3+}-activated $ScCaO(BO_3)$ blue-cyan phosphor with high efficiency toward full-spectrum white LED applications, *Mater. Today Chem.*, 2022, **26**, 101030.
6. M. Cai, T. Lang, T. Han, D. Valiev, S. Fang, C. Guo, S. He, L. Peng, S. Cao, B. Liu, L. Du, Y. Zhong and E. Polisadova, Novel Cyan-Green-Emitting Bi^{3+}-Doped $BaScO_2F$, R^+ (R = Na, K, Rb) Perovskite Used for Achieving Full-Visible-Spectrum LED Lighting, *Inorg Chem*, 2021, **60**, 15519-15528.
7. D. Liu, X. Yun, G. Li, P. Dang, M. S. Molokeev, H. Lian, M. Shang and J. Lin, Enhanced Cyan Emission and Optical Tuning of $Ca_3Ga_4O_9:Bi^{3+}$ for High-Quality Full-Spectrum White Light-Emitting Diodes, *Adv. Opt. Mater.*, 2020, **8**, 2001037.
8. L. Sun, B. Devakumar, J. Liang, S. Wang, Q. Sun and X. Huang, A broadband cyan-emitting $Ca_2LuZr_2(AlO_4)_3:Ce^{3+}$ garnet phosphor for near-ultraviolet-pumped warm-white light-emitting diodes with an improved color rendering index, *J. Mater. Chem. C*, 2020, **8**, 1095-1103.
9. S. Wu, Y. Fu, Q. Liu, P. Xiong, D. Wang, G. Zhang, S. Yuan and Y. Chen, Obtain full visible spectrum light-emitting diode illumination via bismuth-activated cyan phosphors, *Mater. Today Chem.*,

2022, **23**, 100754.
10. Q. Sun, S. Wang, L. Sun, J. Liang, B. Devakumar and X. Huang, Achieving full-visible-spectrum LED lighting via employing an efficient Ce^{3+}-activated cyan phosphor, *Mater. Today Energy*, 2020, **17**, 100448.
11. J. Zhong, Y. Zhuo, S. Hariyani, W. Zhao, J. Wen and J. Brgoch, Closing the Cyan Gap Toward Full-Spectrum LED Lighting with $NaMgBO_3:Ce^{3+}$, *Chem. Mater.*, 2020, **32**, 882-888.
12. S. You, Y. Zhuo, Q. Chen, J. Brgoch and R.-J. Xie, Dual-site occupancy induced broadband cyan emission in $Ba_2CaB_2Si_4O_{14}:Ce^{3+}$, *J. Mater. Chem. C*, 2020, **8**, 15626-15633.
13. H. Liu, W. Zhang, H. Liang, Q. Zeng, J. Shi and D. Wen, Discovery of a new phosphor via aliovalent cation substitution: DFT predictions, phase transition and luminescence properties for lighting and anti-counterfeiting applications, *J. Mater. Chem. C*, 2021, **9**, 1622-1631.
14. R. Zhang and J.-F. Sun, An efficient perovskite-type $Rb_2CaPO_4F:Eu^{2+}$ phosphor with high brightness towards closing the cyan gap, *J. Alloys Compd.*, 2021, **872**, 159698.
15. Q. Zhang, X. Wang and Y. Wang, Design of a broadband cyan-emitting phosphor with robust thermal stability for high-power WLED application, *J. Alloys Compd.*, 2021, **886**, 161217.
16. Y. Zhuo, A. Mansouri Tehrani, A. O. Oliynyk, A. C. Duke and J. Brgoch, Identifying an efficient, thermally robust inorganic phosphor host via machine learning, *Nat Commun*, 2018, **9**, 4377.
17. X. Zhang and J.-F. Sun, Intense blue emission of perovskite-type fluoride phosphor $Cs_4Mg_3CaF_{12}$: Eu^{2+} as a promising pc-WLEDs material, *J. Alloys Compd.*, 2020, **835**, 155225.
18. M. Tian, P. Li, Z. Wang, Z. Li, J. Cheng, Y. Sun, C. Wang, X. Teng, Z. Yang and F. Teng, Controlling multi luminescent centers via anionic polyhedron substitution to achieve single Eu^{2+} activated high-color-rendering white light/tunable emissions in single-phased $Ca_2(BO_3)_{1-x}(PO4)_xCl$ phosphors for ultraviolet converted LEDs, *Chem. Eng. J.*, 2017, **326**, 667-679.
19. S. Wang, Y. Wu, Y. Fan, L. Wu and J. Yu, Crystal structure and photoluminescence properties of blue-green-emitting $Ca_{1-x}Sr_xZr_4(PO_4)_6$: Eu^{2+} ($0\leq x\leq 1$) phosphors, *Mater. Res. Bull.*, 2020, **125**, 110781.
20. J. Qiao, L. Ning, M. S. Molokeev, Y. C. Chuang, Q. Liu and Z. Xia, Eu^{2+} Site Preferences in the Mixed Cation $K_2BaCa(PO_4)_2$ and Thermally Stable Luminescence, *J Am Chem Soc*, 2018, **140**, 9730-9736.
21. J. Tang, J. Si, G. Li, T. Zhou, Z. Zhang and G. Cai, Excellent enhancement of thermal stability and quantum efficiency for $Na_2BaCa(PO_4)_2:Eu^{2+}$ phosphor based on Sr doping into Ca, *J. Alloys Compd.*, 2022, **911**, 165092.
22. J. Xiang, J. Zheng, Z. Zhou, H. Suo, X. Zhao, X. Zhou, N. Zhang, M. S. Molokeev and C. Guo, Enhancement of red emission and site analysis in Eu^{2+} doped new-type structure $Ba_3CaK(PO_4)_3$ for plant growth white LEDs, *Chem. Eng. J.*, 2019, **356**, 236-244.
23. Z. Song, Q. Liu, Effects of neighboring polyhedron competition on the 5d level of Ce^{3+} in lanthanide garnets, *J. Phys. Chem. C* 2019, **123**, 8656-8662.
24. Z. Song, Q. Liu, Structural indicator to characterize the crystal-field splitting of Ce^{3+} in garnets, *J. Phys. Chem. C* 2020, **124**, 870-873.
25. P Dorenbos, Crystal field splitting of lanthanide 4f(n-1)5d-levels in inorganic compounds, *J. Alloy. Compd.,* 2002, **341**,156-159.
26. S. Wang, Z. Song, Y. Kong, Z. Xia, Q. Liu, Crystal field splitting of 4f(n-1)5d-levels of Ce^{3+} and Eu^{2+} in nitride compounds, *J. Lumin.*, 2018,**194**,461-466.
27. P. Dai, Q. Wang, M. Xiang, T.-M. Chen, X. Zhang, Y.-W. Chiang, T.-S. Chan and X. Wang, Composition-driven anionic disorder-order transformations triggered single-Eu^{2+}-converted high-color-

rendering white-light phosphors, *Chem. Eng. J.*, 2020, **380**, 122508.
28. S. Zhang, Y. Nakai, T. Tsuboi, Y. Huang and H. J. Seo, Luminescence and Microstructural Features of Eu-Activated $LiBaPO_4$ Phosphor, *Chem. Mater.*, 2011, **23**, 1216-1224.
29. W. Ji, S. Wang, Z. Song and Q. Liu, Luminescent thermal stability and electronic structure of narrow-band green-emitting Sr-Sialon:Eu2+ phosphors for LED/LCD backlights, *J. Alloys Compd.*, 2019, **805**, 1246-1253.
30. W. Wang, M. Tao, Y. Liu, Y. Wei, G. Xing, P. Dang, J. Lin and G. Li, Photoluminescence Control of UCr_4C_4-Type Phosphors with Superior Luminous Efficiency and High Color Purity via Controlling Site Selection of Eu^{2+} Activators, *Chem. Mater.*, 2019, **31**, 9200-9210.
31. W. Wang, H. Yang, M. Fu, X. Zhang, M. Guan, Y. Wei, C. C. Lin and G. Li, Superior thermally-stable narrow-band green emitter from Mn^{2+}-doped zero thermal expansion (ZTE) material, *Chem. Eng. J.*, 2021, **415**, 128979.
32. Y. Chen, F. Pan, M. Wang, X. Zhang, J. Wang, M. Wu and C. Wang, Blue-emitting phosphor $Ba_4OCl_6:Eu^{2+}$ with good thermal stability and a tiny chromaticity shift for white LEDs, *J. Mater. Chem. C*, 2016, **4**, 2367-2373.
33. J. Liang, B. Devakumar, L. Sun, S. Wang, Q. Sun and X. Huang, Full-visible-spectrum lighting enabled by an excellent cyan-emitting garnet phosphor, *J. Mater. Chem. C*, 2020, **8**, 4934-4943.
34. Z. Zhang, B. Devakumar, S. Wang, L. Sun, N. Ma, W. Li and X. Huang, Using an excellent near-UV-excited cyan-emitting phosphor for enhancing the color rendering index of warm-white LEDs by filling the cyan gap, *Mater. Today Chem.*, 2021, **20**, 100471.
35. W. Li, N. Ma, B. Devakumar and X. Huang, Blue-light-excitable broadband yellow-emitting $CaGd_2HfSc(AlO_4)_3:Ce^{3+}$ garnet phosphors for white light-emitting diode devices with improved color rendering index, *Mater. Today Chem.*, 2022, **23**, 100638.
36. S. He, F. Xu, T. Han, Z. Lu, W. Wang, J. Peng, F. Du, F. Yang and X. Ye, A Mn^{4+}-doped oxyfluoride phosphor with remarkable negative thermal quenching and high color stability for warm WLEDs, *Chem. Eng. J.*, 2020, **392**, 123657.
37. N. C. George, A. Birkel, J. Brgoch, B.-C. Hong, A. A. Mikhailovsky, K. Page, A. Llobet and R. Seshadri, Average and Local Structural Origins of the Optical Properties of the Nitride Phosphor $La_{3-x}Ce_xSi_6N_{11}$ ($0 < x \leq 3$), *Inorg. Chem.*, 2013, **52**, 13730-13741.
38. Z. Sun, B. Sun, X. Zhang, D. Wen and P. Dai, Superb thermal stability purple-blue phosphor through synergistic effect of emission compensation and nonradiative transition restriction of Eu^{2+}, *Mater. Today Chem.*, 2022, **24**, 100877.
39. S. Yang, Y. Wu, F. Yue, R. Qi, B. Jiang, J. Wu, Y. Shen, C. Duan, Y. Shan, Q. Zhao and Y. Zhang, $MGa_2B_2O_7:Bi^{3+},Al^{3+}$ (M = Sr, Ba) blue phosphors with a quantum yield of 99% and negative thermal quenching, *Inorg. Chem. Front.*, 2021, **8**, 4257-4266.
40. H. Yang, P. Li, X. Fu, Z. Ye, X. Huo, Y. Wang, Q. Wu, H. Suo, L. Li and Z. Wang, A novel blue emitting phosphor $LaScO_3:Bi^{3+}$ for white LEDs: high quantum efficiency, high color purity and excellent thermal stability, *Mater. Today Chem.*, 2022, **26**, 101050.